ACS OMEGA

Open Access

http://pubs.acs.org/journal/acsodf

Article

OH-Impregnated Household Bleach-Making Sediments for the Catalysis of Waste Cooking Oil Transesterification: Parameter Optimization

Kedir Derbie Mekonnen* and Anwar Yimer Yesuf

Cite This: *ACS Omega* 2024, 9, 4613−4626

Read Online

ACCESS | Metrics & More | Article Recommendations | Supporting Information

ABSTRACT: Industrial and academic societies have been bothered with the generation and subsequent management of residues settled out from household bleach, due to its corrosive properties. Therefore, the aim of this research was to introduce a NaOH-impregnated calcium-based solid catalyst from the aforementioned sediments for waste cooking oil transesterification. To prepare the catalyst (RC-ITB), the wet impregnation technique was followed and successfully characterized via X-ray diffraction (XRD), X-ray fluorescence(XRF), differential scanning calorimetry (DSC), Brunauer−Emmett−Teller (BET), Fourier transform infrared (FT-IR), and scanning electron microscopy (SEM) methods. The study findings suggested that RC-ITB has a BET surface area of 9.312 m^2 g^{-1} and is largely made up of calcium with its compound forms such as carbonates, hydroxides, and oxides. The evaluation of pH values verified that RC-ITB is more alkaline (i.e., pH = 12.65) relative to its precursor RC (pH = 10.66), largely attributable to OH impregnation. To study the catalytic performance, three numeric factors with three levels of treatment were used, and their influences were analyzed through a response surface approach. Accordingly, the optimal yield of biodiesel was found to be 80.04% at a reaction temperature of 61 ± 2 °C, catalyst weight of 6.33 wt %, and a molar ratio of 23.94. Moreover, FTIR analysis verified that the glycerol part of triglycerides had been replaced with a methoxyl unit. Also, the fuel quality parameters of the FAME product were examined, including density, kinematic viscosity, acid value, density, cetane number, cloud point, saponification value, and pour point; all of these values fall within the ASTM D6751-accepted limits. Thus, the findings showed that the sediments of household bleach production could be a candidate source to explore heterogeneous basic catalysts.

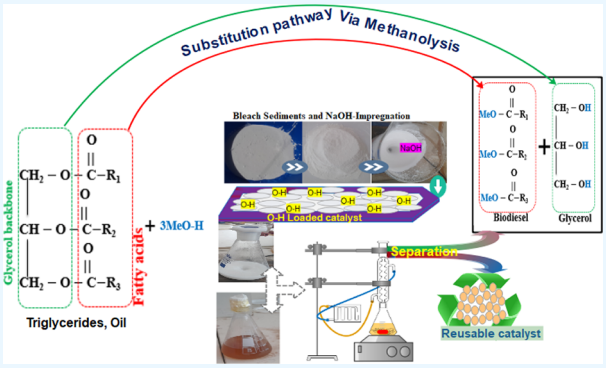

INTRODUCTION

Energy is one of the essential requirements for playing a prominent role in the power generation, transportation, and industrial sectors. Fossil fuels, including natural gas, coal, and petroleum, provide the majority of energy utilized worldwide. These resources, however, are finite, hazardous, and eventually run out. Thus, the development of biofuel such as biodiesel that can be a viable alternative to the desired fuel supply has attractively increased worldwide interest and could be a novel technology.[1,2] Biodiesels have several benefits over resources because of their properties like nontoxic nature, biodegradable, and high flash points, mixed with diesel because of their similar features, less CO emissions, and high cetane number.[2,3] However, 70−95% production cost of biodiesel is governed by the price of the organic raw material. Thus, the third-generation feedstock, waste cooking oils such as palm oil, is commonly used as the low-priced alternative feedstock in addition to the second-generation nonedible vegetable oils.[3] The waste-cooking-palm-oil's major fatty acid constituents include oleic (C18:1), linoleic (C18:2), palmitic (C16:0), lauric (C12:0), myristic (C14:0), and stearic (C18:0).[4] Apart from low-cost substrates, the kind of catalysts employed in the process of transesterification also determines the cost of biodiesel synthesis.[3,5] Ordinarily, transesterification reactions are catalyzed with alkaline-homogeneous catalysts because of a better yield in shorter periods under mild conditions. However, the system needs a lower free fatty acid plus moisture level of the raw material <0.5% and <0.1%, respectively, otherwise homogeneous acid catalysts are used.[6−8] Although homogeneous catalysts have numerous drawbacks like saponification at larger free fatty acid levels, difficulty in phase separation, nonreusability, washing and drying requirement, and thus could raise the generation of wastewater plus total costs of

Received: October 7, 2023
Revised: December 22, 2023
Accepted: January 8, 2024
Published: January 22, 2024

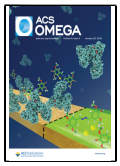

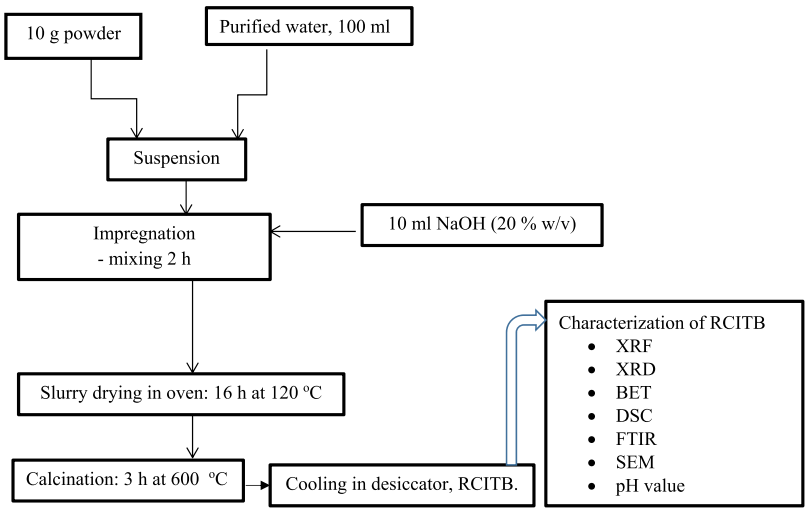

Figure 1. Block flow diagram for wet impregnation and calcination process of RC-ITB.

production.[8−11] Hence, the use of heterogeneous catalysts could be a noble alternative to the homogeneous one because of their reusability, separation easiness, low environmental and corrosion problems, and avoid pre-esterification of high acidic feed stocks.[6,10,12] Such heterogeneous catalysts could be either acidic or alkaline. However, solid alkaline catalysts are usually used in the transesterification process compared to the acidic one because acid heterogeneous catalyzed reaction exhibits a variety of demerits, such as a high catalyst amount requirement, higher methanol molar ratio, high reaction temperature, and slow reaction. Thus, alkaline solid-state catalyst advancement, classically calcium-based, is the current interesting theme of many researchers. Since calcium-based catalysts usually have high alkaline natures, the numerous agricultural and industrial waste materials, for example, cement wastes, bones, waste eggshells, etc., are utilized to provide CaO catalysts having catalysis abilities.[11−15] However, the catalytic activity of heterogeneous catalysts is usually lower than homogeneous catalysts due to the dual effects of mass transfer limitation and low alkalinity. To improve this limitation, alkaline solid catalysts are ordinarily infused with NaOH and KOH aiming to load more OH ions on the catalyst surface, which in turn increases the catalyst's basic strength essential for better catalytic capability.[8,16,17] In this work, liquid bleach-making from $Ca(ClO)_2$ results in liquidate precipitates as a byproduct product, which can be accepted as a novel idea for solid catalyst making through alkaline impregnation. Calcium hypochlorite is the active constituent for bleach production, functionally boosting material whiteness by stripping any unwanted coloring things.[18−23] Industrially, the calcium-rich precipitate is settled out from the liquid form bleach-making and is often rid of as trash. However, its uncontrolled removal might contribute to serious human health and environmental problems due to its hazardous and corrosive nature.[20,22] As a result, industrial and academic societies have been faced with finding a means of its utilization. Therefore, the aim of this study was to develop a NaOH-impregnated Ca-based heterogeneous catalyst from the above-mentioned precipitates by knowing its composition for biodiesel synthesis, which is crucial for the integration of industrial resources as well as for the preservation of the environment.

MATERIALS AND METHODS

Materials. As a biodiesel feedstock, waste cooking palm oil was gathered from nearby pan-fried chips vendors. To be a catalyst, sediments of liquid bleach made of $Ca(OCl)_2$ were received from an indigenous business owner (Robi Soap industry) in Kombolcha, Wollo, Ethiopia. In this particular experiment, all reagents and chemicals employed were analytical grade (Refer to the Supporting Information for lists of chemicals and equipment).

Methods. *WCO's Free Fatty Acid Content and Saponification Value.* First, suspended solid impurities and food residuals from the crude waste cooking oil (WCO) were removed by heating at 90 °C for 1 h, followed by filtration,[24−26] and stored in a sealed clean container. Then, AOAC-1990 and ASTN-D664 standard protocols were followed to find the SV and FFA contents of WCO, respectively. Lastly, the WCO molecular weight was predicted from the aforementioned values via eq 1.[24] To test the suitability of WCO for homogeneous catalysis system, a methanolysis reaction with NaOH was used (Figure S1 in the Supplementary Data).

$$MW_{,wco} = \frac{56.1 \times 1000 \times 3}{(SV - AV)} = \frac{168,300}{(SV - AV)} \quad (1)$$

Catalyst Preparation and Characterization. The collected semisolid state precipitates were sun dehydrated for 4 days and subsequently dried for 3 h in the oven at 110 °C. Then, the size reduction of the dried precipitate was made via mortar and sieved to below 355 μm size.[11,24,27] Then, the catalyst was prepared by applying the wet impregnation method with NaOH, followed by calcination (based on Figure 1), aiming to load more OH ions on the surface needed to hasten the reaction rate.[8,10,16,24] Calcination is a crucial step in the morphological evolution of the catalyst surface because it removes volatile components and releases moisture that has been both chemically and physically bound.[17] All of the pictorial outlooks of the above techniques are shown in Figures S2 and S3 in the Supporting Information. Finally, it was characterized for its elemental composition, phase identification, specific surface area, heat flow variation, surface functional group, and morphological characteristics using X-ray fluorescence (XRF), X-ray diffractometry, Brunauer−

https://doi.org/10.1021/acsomega.3c07810
ACS Omega 2024, 9, 4613−4626

Emmet−Teller method (BET), differential scanning calorimetry (DSC), Fourier transform infrared spectroscopy (FTIR), and scanning electron microscopy (SEM), respectively, as illustrated in the Supporting Information. In addition, the basic nature of RC-ITB in comparison to its precursor coded with RC was evaluated by pH value measurements via pH meter (PHS-3C). The measurements were made by making six different solutions for 1 g of catalyst in 5, 10, 15, 20, 25, 30, 35, and 40 mL of distilled water.[28,29]

Transesterification of Waste Cooking Palm Oil. *Experimental Design.* Table 1 shows the experimental design

Table 1. Experimental Domain with Natural and Coded Values of Independent Variables Used in Box-Behnken Design (BBD) for Transesterification Reaction

			coded variable level		
variable	unit	symbol/code	level 1 −1	level 2 0	level 3 +1
reaction temperature	°C	A	55	65	75
methanol-to-oil molar ratio		B	10	20	30
catalyst loading	wt %	C	3	6	9

for three numeric factors on the three levels of treatment was done by applying the Box-Behnken experimental design of response surface methodology (RSM) to study their effects on the response and FAME yield. The combinations of these three independent variables generate 17 randomized runs while maintaining a 1 h reaction time and 600 rpm stirring rate in support of literature. Lastly, the reaction processes' yield of FAME was computed (eq 2).

$$\%\text{FAME yield}, \quad Y = \frac{\text{gram of produced biodiesel}}{\text{gram of oil sample used for the reaction}} \times 100\% \tag{2}$$

Experimental Setup and Procedure. The synthesis of fatty acid methyl ester (FAME) from waste cooking palm oil was performed using the setup presented in Figure 2. The reaction process was carried out by reacting preheated oils at the desired reaction temperature and methanolic predissolved catalysts in a borosilicate glass reactor fitted with a reflux condenser at a fixed time and mixing rate using the magnetic bar. Subsequently, a WKM centrifuge operated at 3500 rpm was used to separate the reaction mixtures from the solid catalyst, and phase separation of biodiesel with glycerol was made by settling in the funnel for 12 h, i.e. glycerol at the bottom and FAME at the top. Then, separation of the free unreacted methanol from the FAME products was made by rotary evaporator, consequently drying at 110 °C in the oven to remove trace methanol and moisture if any.

Analysis of Data and Parameter Optimization. To assess the effects of particular reaction parameters, the importance of experimental results from the response surface methodology (RSM) design matrix was examined, which includes all interaction factors and optimized through the use of a fitted polynomial second-order model expression (eq 3).

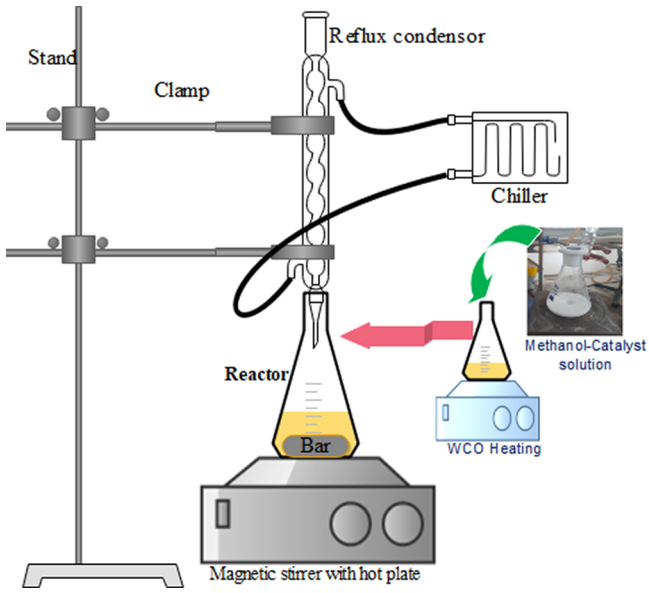

Figure 2. Experimental setup.

$$\text{Yield}, \quad Y = B_0 + \sum_{i=1}^{3} B_i X_i + \sum_{i=1}^{3} B_{ii} X_i^2 + \sum_{i}^{2} \sum_{i<j}^{3} B_{ij} X_i X_j \tag{3}$$

where Y is the dependent variable (yield of methyl ester); X_i and X_j are the i^{th} and j^{th} coded independent variables; B_0, B_i, B_{ii}, and B_{ij} respectively denote the intercept, linear, quadratic, and interaction effect regression coefficients.

For optimization purposes, the values of dependent and independent variables to be predicted from the model were verified by triple tests.

Catalyst Reusability Test. The RC-ITB catalyst separated from the reaction mixture under the optimum reaction conditions was subjected to its reusability test via a continual reaction of 4 cycles without any treatment.

Biodiesel Quality and FT-IR Analysis. Standard procedures have been employed to examine the biodiesel fuel qualities produced from WCO: Standard procedures have been employed to examine the biodiesel fuel qualities produced from WCO: ASTM-D 5853 (pour point), ASTM-D 1298 (density), ASTM-D 4737 (cetane number), ASTM-D 664 (acid value), ASTM-D 2500 (cloud point), AOAC-1990 (saponification value), and ASTM-D445 (flow resistance and viscosity). Analysis of biodiesel with FTIR spectroscopy was done to confirm the FAME formation from the substrate caused by replacement via transesterification reaction. In this method, the liquid sample was first sandwiched between two well-cleaned KBr disks, and biodiesel spectra were generated at a scanning speed and resolution of 2 mm s^{-1} and 4 cm^{-1}, respectively, in between 400 and 4000 cm^{-1} wave number.

RESULTS AND DISCUSSION

WCO's Saponification Number and Free Fatty Acid Content. To decide the techniques of using a heterogeneous or homogeneous catalysis system, knowing the free fatty acid level of the feedstock is very important. The permissible FFA amount for the homogeneous catalysis process is typically below 2.5%; otherwise, saponification may be favored and the production of biodiesel could be diminished. Also, a greater saponification value represents its suitability for soap formation

https://doi.org/10.1021/acsomega.3c07810
ACS Omega 2024, 9, 4613−4626

and abundance of fatty acids with a reduced molecular weight in large quantities. The saponification value of various biodiesel feedstock ranges between 130 and 193 mg KOH/g.[5,30] However, experimental values of FFA and SV respectively were 16.31% and 223.403 mg KOH/g, which exceed the suggested values. Hence, the use of heterogeneous catalysts as a substitute for homogeneous catalysts is rationally established. Moreover, the unsuitability of the homogeneous catalysis was confirmed with NaOH catalyst for WCO transesterification, and solid soap product was observed (Figure S1 in the Supporting Information).

Characterization of RC-ITB Catalyst. *X-ray Fluorescence Analysis.* The XRF analysis shows that the prepared catalyst contains a Ca (~64.27%) element with its corresponding oxide form, CaO (~89.92%), as a major composition, which could be a promising base catalyst in the synthesis of biodiesel. Also, other metal oxides in a minor amount were detected, such as silicon dioxide (SiO_2, 6.45%), aluminum oxide (Al_2O_3, 1.95%), ferric oxide (Fe_2O_3, 0.14%), potassium oxide (K_2O, 0.096%), and phosphorus pentoxide (P_2O_5, 0.000997%). It is widely recognized that the aforementioned oxides are the transesterification reaction's active ingredients.[31] The detail of each composition is presented in the Supporting Information (Table S1).

X-ray Diffraction Analysis. The crystalline phases of the RC-ITB catalyst and its precursor, RC (raw dried precipitate), were determined by a diffraction angle position of 2θ between 10−80°. Usually, the width of the peak is inversely proportional to the crystal size. A larger crystal has a thinner peak, while the smaller crystals have a broader peak because of defects in the structure or amorphous nature (absence of perfect crystallinity). As shown in Figure 3, the main candidate

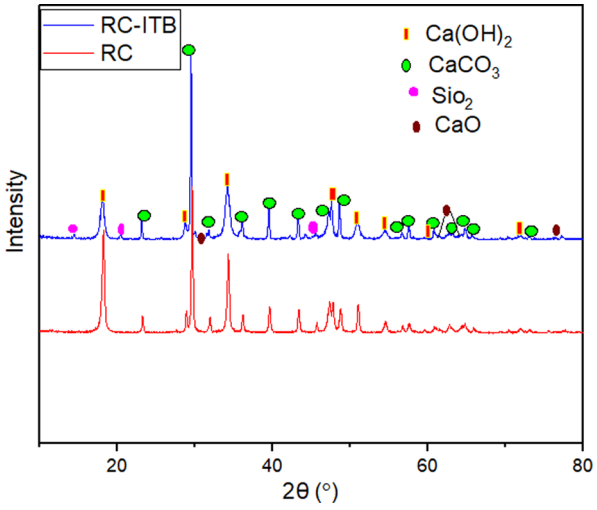

Figure 3. XRD analysis of the RC-ITB (blue) and RC (red).

phases within the two forms were similar, and the peak-match application was implemented to distinguish them from XRD diffraction peak patterns. The matched phase of portlandite, $Ca(OH)_2$, was located at the 2θ degree value of 34.24, 18.12, 47.66, 28.76, 50.9, 59.56, 54.52, and 71.64°, while the $CaCO_3$(calcite) crystalline phases at 43.32, 29.52, 31.84, 36.1, 23.2, 39.52, 57.54, 48.62, 56.69, 60.8, 63.2, 64.2, 73.02, and 47.26°. CaO was perceived at 2θ = 75.98, 30.89, 61.46, and 64.26°. SiO_2 at 45.56,14.47, and 20.44°. The high contents of Portlandite and calcite may be the result of carbonation and/or hydroxylation of the combustion product, CaO, with ambient moisture and CO_2 in the atmosphere to form a permanent polymorph of them. calcite and Portlandite, respectively.[13,32,33] These compounds are the primary components that make up basic catalysts, which can be detected in XRD analysis. With the exception of portlandite and calcite phases, other elements known with XRF were detected at nonperfect peaks with a very low value of FOM, which may be attributable to their amorphous nature or quantitative insensitivity of the XRD machine as proved in the software. The absence of crystalline phase variations between RC and RC-ITB was reasonably due to the lower thermal treatment of RC-ITB during the calcination process.

Differential Scanning Calorimetry Analysis. Differential scanning calorimeter (DSC) infers the variation of heat flow involved in the exothermic processes−the release of heat (negative ΔH, calorific value), and/or endothermic process−the absorption of heat (positive ΔH, needed for evaporation of moisture and release of volatile matters in a nitrogen atmosphere).[34,35] The DSC analysis result of the RC-ITB catalyst is shown in Figure 4. The wide beaks at around 47

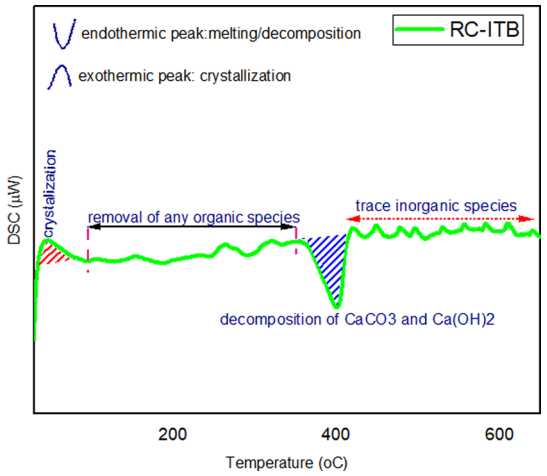

Figure 4. DSC analysis of the RC-ITB catalyst.

°C on the DSC thermogram are ascribed to the removal of many unbounded moistures from the catalyst surface and initiation of crystallization through heat removal. The lower endothermic/exothermic inflection points in the temperature range between 95 and 350 °C could be resulted from the removal of residual moistures and unstable carbonaceous compounds(organic components) adhered on the surface of the catalyst which are not removed during the processing.[26,35] The dipper and wider peak at around 400 °C is attributed to the breakdown of many of the metal carboxylate compounds like $CaCO_3$ and $Ca(OH)_2$;[35] such species were attractively confirmed in the XRD analysis. The subsequent low areas of sinusoidal wavelike endothermic and exothermic peaks could be linked with the decomposition and/or crystallization of remaining carboxylate compounds as well as other inorganic crystal phases detected in XRD, for instance, SiO_2, Al_2O_3, and Fe_2O_3.

BET Surface Area Analysis. The Brunauer−Emmett−Teller inspection showed that the specific surface area of the RC-ITB is about 9.312 $m^2\ g^{-1}$ while a reduced BET result of 8.509 $m^2\ g^{-1}$ was observed on the raw untreated form (RC) due to the presence of various impurity attachments

https://doi.org/10.1021/acsomega.3c07810
ACS Omega 2024, 9, 4613−4626

accountable for surface pore blockage. Generally, the BET outcome implies that the prepared impregnated catalyst is expected to have better active sites essential for enhanced catalysis capacity and could be competent with other catalysts developed from different sources as set out in Table 2. The difference between these results may be due to the nature of the material, particle size, and activation conditions.

Table 2. BET Surface Area of the RC-ITB Catalyst Compared with Other Findings

source of catalyst	BET surface area ($m^2\ g^{-1}$)	reference
RC-ITB	9.312	this study
biomass fly ash	9.0280	32
eggshell ash	30.7	31
walnut shell ash	8.8	36
eggshell nanocatalyst	8.0142	37
calcined commercial $CaCO_3$	1.7364	
KNO3-loaded coffee husk ash	2.251	24

Fourier Transform Infrared Spectroscopy Analysis. As shown in Figure 5, FTIR was used to locate the chemical

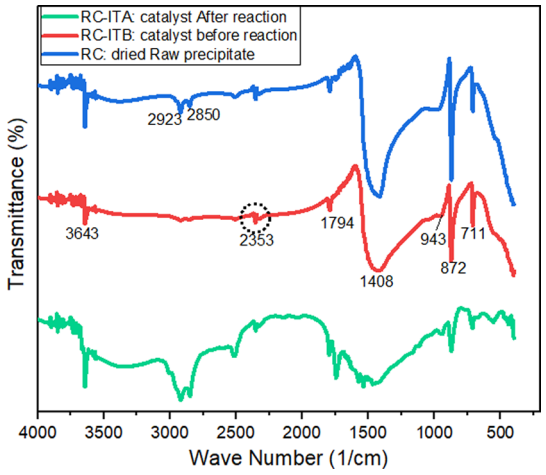

Figure 5. FTIR spectra of RC (blue), RC-ITB (red), and RC-ITA (green).

groups on the synthesized catalyst's surface, RC-ITB, in combination with its after-reaction phase (RC-ITA), and the pioneer dried raw precipitate (RC) were identified. With the exception of physisorbed water molecules occurring at 2923 and 2850 cm^{-1} due to O−H stretching of the − H on RC, the patterns of RC-ITB and RC are nearly analogous; the nonexistence of such unique bands on RC-ITB might be rationally eliminated through the calcination temperature due to weak surface bonds. The other O−H bond stretching modes of $Ca(OH)_2$ were observed at about 3643 and 1794 cm^{-1} in both samples, either naturally on the RC or due to the adhered moistures on the calcinated product surface to form Portlandite. Wave number at 1408 cm^{-1} shows the asymmetric stretching vibrations of C−O bonds in carbonate ions (CO_3^{2-}) due to the presence of $CaCO_3$ and/or the surrounding carbon dioxide chemisorption throughout the catalyst's surface. Similarly, the bending stretching mode of the C−O bond symmetrically within calcareous compounds has been identified to exhibit both out-of-plane as well as in-plane vibrations at 872 and 711 cm^{-1}, respectively; 943 cm^{-1} is the distinctive band of Si−O bond.[8,10,32,33,38,39] All of the aforementioned compounds were prettily identified with XRF and XRD analysis. Moreover, the impregnation effects of the catalyst are observed around 2323 cm^{-1}enabling the evolution of a new, substantial O−H binding that remained stable through the conditions of calcination because of the strong chemical attachment properties on the RC-ITB catalyst, while elimination could be possible on the RC one due to the physisorbed nature. Furthermore, the new peaks of RC-ITA (after reaction) observed at around 2922, 2847, 2510, 1748, and 1537 and the wider curve between 1689 and 992 cm^{-1} all arise from the build-up of organic contaminants that result from oil reactivity on the catalyst site; their corresponding chemical group is similar to the oil and FAME spectra, as depicted in Figure 12. Such impurities have a negative effect on the catalyst performance for further usage due to the loss of its active sites.

Scanning Electron Microscopy Analysis. The surface microstructure and morphology of materials are usually analyzed with scanning electron microscopy. Figure 6 represents the surface structural variation between the SEM micrographs of RC-ITB and RC-ITA combined with RC and PC (pure grade CaO, 99.5% rankem brand), aiming for ease of structural implications. Figure 6a designates the numerous well-formed lump of fogs-like organization of the SEM image patterns of the reference catalyst (CaO), which infers its permeable crystalline arrangement necessary for providing improved active areas so that reactions can take place.[8,40] Due to the presence of impurities associated with the untreated surface of the RC (Figure 6b), the varying sizes of surface structural patterns of RC-ITB (Figure 6c) are more apparent to PC (reference), because of the dual alkaline and heat treatments needed to provide enhanced active areas preferred for response hastening.[8] The topography of the RC-ITA phase is presented in Figure 6d, and the result notably indicates the amorphous-like porous structure reasonably due to the buildup of oil impurities on the catalyst surface liable to block its active sits.[41]

Determination of the pH Value. The variations of pH values of RC and RC-ITB with the various levels of distilled water are depicted in Figure 7. It can be seen that the pH drops linearly as the volume of the thinning solvent is enlarged, i.e., from 12.65 to 11.92 (RC-ITB), and 10.66 to 9.83 (RC), this could be linked with the contribution to neutralization at higher volumes thereby reducing the pH levels. For similar volumes of water, RC-ITB has a higher pH value than RC, which logically arises from the alkaline infusion liable to improve its basic nature, which is very important for improved catalysis of the reaction medium.

Response Surface Methodology and Fuel property Analysis of Biodiesel Production. *Model Fitting and Adequacy Checking.* The response surface methodology (RSM) contains a group of statistical techniques that want to show the sound effects of parameters on the desired response via a quadratic model equation. Upon the experimental parameter combinations, the actual percentage yields of FAME from WCO with its corresponding predicted values including residuals are shown in Table 3.

Based on the result, the RSM under design expert provided a "suggested quadratic model," as shown in Table 4, having insignificant lack-of-fit p-value (0.2254 > 0.05) from the model alternatives (linear, two-factor interaction (2FI), quadratic and cubic polynomial).

https://doi.org/10.1021/acsomega.3c07810
ACS Omega 2024, 9, 4613−4626

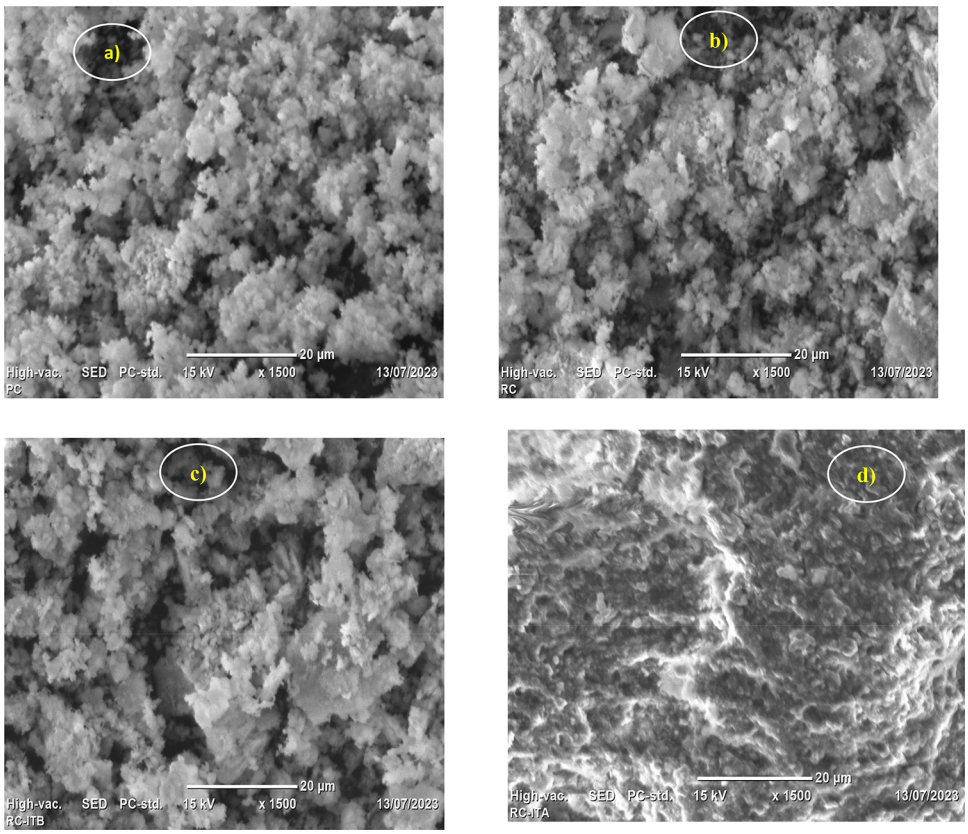

Figure 6. SEM analysis of PC (a), RC (b), RC-ITB (c), and RC-ITA (d).

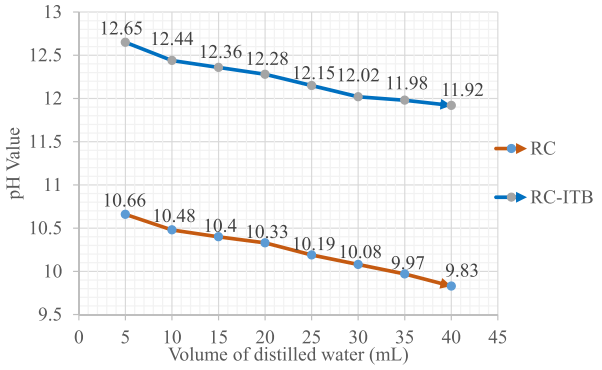

Figure 7. pH value variation of RC and RC-ITB (1 g) dissolved in numerous volumes of water.

To evaluate the significance and fitness of the quadratic model along with individual terms as well as their interaction effect on the responses, statistical analysis was executed using analysis of variances (ANOVA) with the help of probability error value (p-value) as shown in Table 5. A particular model term is statistically significant when p-values ≤ 0.05, else insignificant ($P > 0.05$); the smaller the p-value, the more the significance.

From the ANOVA result, it can be observed that the "Model F-value" of 1001.90 implies the relevance of the model; there is just a 0.01% probability that the larger F-value may occur because of noise. All model terms A, B, C, D, AB, AC, BC, A^2, B^2, and C^2 are important since their p-values are less than 0.05. The F-value of lack-of-fit (2.24) with a p-value of 0.2254 suggests that the lack-of-fit is not substantial compared to the pure-error. There is a 22.54% chance that a Lack of Fit F-value this large could happen due to noise. A nonsignificant lack-of-fit is an excellent way to demonstrate how well the model and experimental data fit together. Using the coded elements (A, B, and C), the regression model equation used to predict the response variable can be expressed by eq 4.

$$\text{FAME Yield: } +78.54 - 5.78A + 6.96B + 4.52C + 1.37AB + 7.60AC + 1.52BC - 6.90A^2 - 8.59B^2 - 12.82C^2 \quad (4)$$

Furthermore, the model's adequacy in explaining how the FAME yield varies with the chosen factors may be evaluated through using the 3-R^2 values generated from the ANOVA result. Coefficients of determination (R^2) assess how much a predictor variable influences a dependent variable, whereas adjusted and predicted R^2 measures the degree to which the model explains variance "around the mean" and "in the new data," respectively. The value of R^2 (0.9992) is near unity, and the variation between Adjusted R^2 (0.9982) and predicted R^2 (0.9918) smaller than 0.2 is desirable to show the existence of good fitting between the experimental data and the model. Also, the signal-to-noise ratio is measured by Adeq Precision. A ratio of 95.115 suggests an adequate signal because a ratio larger than 4 is desired. A model with a lack of fit implies the relationship between the independent and dependent variables is not adequately described because of the presence of large residuals (difference between the predicted and observed response) or major terms are missed when fitting the model. In addition, the reduced standard deviation level (0.5157) and Coefficient of Variation (0.7908%) show the accuracy of the model used to navigate the design space.

https://doi.org/10.1021/acsomega.3c07810
ACS Omega 2024, 9, 4613−4626

Table 3. Yield of FAME over RC-ITB

	parameter-1	parameter-2	parameter-3	response (FAME yield)		
run	temperature (A), °C	alcohol:oil molar ratio (B)	catalyst load (C), wt %	actual value, %	predicted value, %	residual value
1	65	30	3	57.66	58.05	−0.39
2	65	20	6	78.21	78.54	−0.33
3	65	20	6	78.88	78.54	0.34
4	55	20	3	68.15	67.67	0.48
5	65	10	9	53.55	53.16	0.39
6	65	20	6	78.69	78.54	0.15
7	65	20	6	77.99	78.54	−0.55
8	65	20	6	78.92	78.54	0.38
9	55	10	6	62.79	63.23	−0.44
10	75	10	6	49.02	48.93	0.09
11	55	20	9	61.58	61.52	0.06
12	65	30	9	70.15	70.12	0.03
13	75	20	3	40.86	40.92	−0.06
14	55	30	6	74.33	74.42	−0.09
15	75	30	6	66.03	65.58	0.45
16	75	20	9	64.67	65.14	−0.47
17	65	10	3	47.13	47.16	−0.03

Table 4. Model Fit Summary

source	lack of fit *p*-value	adjusted R^2	predicted R^2	
linear	<0.0001	0.1890	−0.0223	
2FI	<0.0001	0.1106	−0.3716	
quadratic	**0.2254**	**0.9982**	**0.9918**	**suggested**
cubic		0.9988		aliased

Parametric Effects on the FAME Yield. The effects of the reaction conditions on the FAME yield are depicted in Figures 8 and 9, which can identify the potential differences in variability between variable levels. The ANOVA result indicates that biodiesel yield can be influenced by all of the important variables of the reaction process. Even though the reaction parameters have synergistic and/or antagonistic effects on the response, better FAME yield was achieved at the center point of the predictive variables which are part of the experiment. However, a variable above a certain value may reduce the desired product.

Figure 8a illustrates how the reaction temperature affects FAME production. Moderate temperature is desirable for the rapid reaction rate to have a higher response value because of the reduction of oil viscosity for enhanced mass transfer within the reaction medium. However, the yield of FAME is obviously reduced at higher as well as lower temperature levels. A lower temperature causes a slower reaction rate because of a higher viscosity and poor catalyst dispersion, while a very high temperature contributes to excess methanol loss as well as the reversibility of the reaction.[5,42−44] was obtained at a temperature of about 65 °C. Figure 8b shows the impacts of the methanol-to-oil molar ratio on the conversion of WCO into FAME. Since the transesterification reaction is reversible, the use of increased molar ratio drives the reaction into the product side resulting in a higher desired product in a short time. However, the extreme increase in molar ratios does not

Table 5. ANOVA Results for the Quadratic Model

source	sum of squares	df	mean square	*F*-value	*p*-value	significance
model	2398.11	9	266.46	1001.90	<0.0001	significant
A—temperature	267.61	1	267.61	1006.25	<0.0001	significant
B—molar ratio(Alco:Oil)	387.53	1	387.53	1457.16	<0.0001	significant
C—catalyst weight	163.35	1	163.35	614.22	<0.0001	significant
AB	7.48	1	7.48	28.13	0.0011	significant
AC	230.74	1	230.74	867.59	<0.0001	significant
BC	9.21	1	9.21	34.64	0.0006	significant
A^2	200.55	1	200.55	754.09	<0.0001	significant
B^2	310.98	1	310.98	1169.30	<0.0001	significant
C^2	692.17	1	692.17	2602.63	<0.0001	significant
residual	1.86	7	0.2660			
lack of fit	1.17	3	0.3893	2.24	0.2254	not significant
pure error	0.6939	4	0.1735			
cor total	2399.97	16				
std. dev.	0.5157	R^2			0.9992	
mean	65.21	adjusted R^2			0.9982	
C.V. %	0.7908	predicted R^2			0.9918	
		adeq precision			95.1149	

significant when $p \leq 0.05$, and insignificant when $p > 0.05$

https://doi.org/10.1021/acsomega.3c07810
ACS Omega 2024, 9, 4613−4626

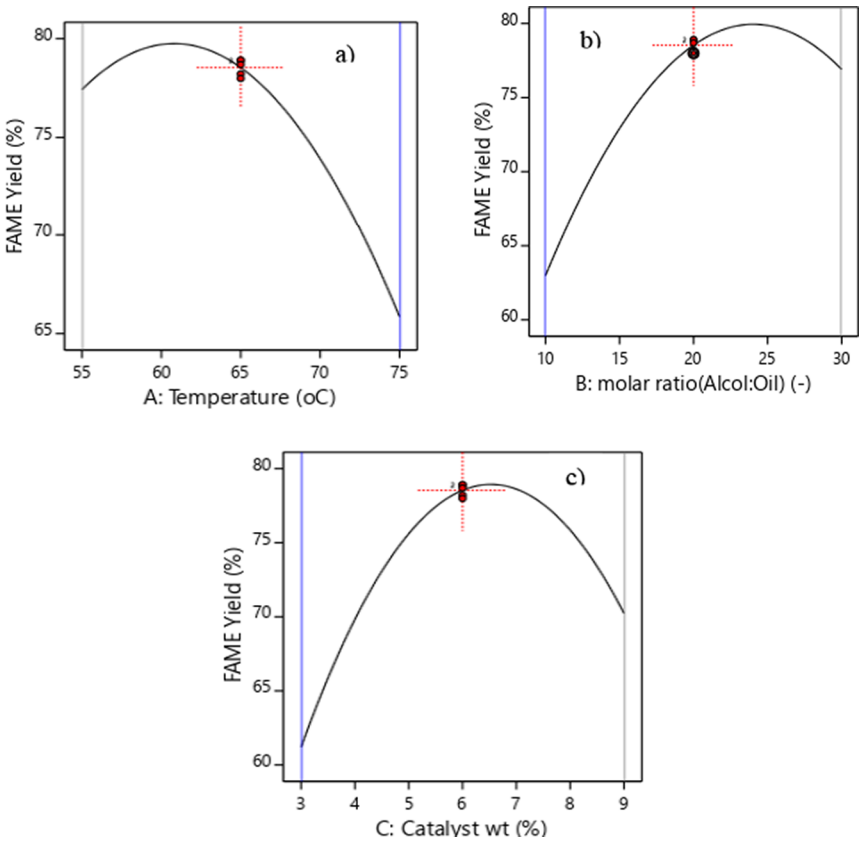

Figure 8. Effects of individual reaction conditions on the FAME yield: (a) temperature; (b) methanol-to-oil molar ratio; (c) catalyst weight.

increase yield, but it improves the solubility of glycerol, which leads to phase separation difficulties and drives the equilibrium back to the left.[45,46] Thus, a higher value of biodiesel yield was obtained at a molar ratio of 20:1. The effect of catalyst weight is also another important factor affecting the transesterification reaction as presented in Figure 8c. The function of the catalyst is to give up sufficient sites of activity so that the reaction is possible. The yield was linearly increased with an increasing amount of catalyst up to the intermediate level because the available active sites can be increased as other catalysts are added, thus facilitating the reaction. However, an extra rise of catalyst results in a decline in yield as a consequence of aggregation of catalysts and the poor mixing of the reaction mixture could be maintained;[31] importantly, since the reaction medium consists of three phases (i.e., oil−methanol−catalyst), the mass transfer effect of solid catalyst is one of the reasons to why the reaction would be slow and does not reach its completion at a higher amount.[42] Thus, a good result was obtained at the catalyst load of 6 wt %.

Furthermore, the interaction plots of independent parameters for the FAME yield are presented in both the 3D surface and contour plots, as shown in Figure 9a−c and d−f, respectively. Plotting the response variable against various combinations of numerical elements in two dimensions to illustrate the relationships between them is called a contour plot. Whereas, the 3D surface is a projection of the contour plot, providing shapes for two independent variables' functional relationships with the dependent one. Although all three interaction terms were significant, the great influence of catalyst dosage with temperature combination on the FAME yield was perceived from the result (Figure 9a,d) compared to the other mutual effects (Figure 9b,c) in support of ANOVA analysis. This is due to the fact that a sufficient catalyst amount for sufficient active sites with a suitable temperature level for better mass transfer is required for improved ester yield.

Optimization of Reaction Conditions and Confirmation. Finding the best possible combinations of reaction conditions is the aim of optimization in order to boost the desired product, the FAME yield. As shown in Figure 10, variables at the cur points that mutually optimize the response have been generated under the response optimizer of RSM via Minitab-17 software on the numeric optimization criteria with its desirability. Consequently, the predicted values for each independent variable between their high and low levels were about 61.87 °C temperature, 23.94 molar ratio, and 6.33 wt % catalyst load for an enhanced response of 81.06% with desirability of 1.

To confirm the predicted results, triplicate experiments were carried out, and an average value was reported, as shown in Table 6. Accordingly, the average actual result of 80.04% was achieved, which is close to the model-based-estimated FAME yield (81.06%) exhibiting a minimal error of percentage (1.02%); this indicates that the generated model provided sufficient predictability of biodiesel yield under the test conditions used. Therefore, the model implemented may possibly describe the transesterification reaction using NaOH-impregnated $Ca(ClO)_2$ precipitate as a heterogeneous catalyst.

Moreover, the comparison of the current study findings with the contributions of other scholars is presented in Table 7. Each heterogeneous catalyst is known to have a distinct precursor that affects how the catalyst behaves as it is produced. Consequently, the activity and quality of solid-state catalysts are significantly influenced by the activation conditions and catalyst source composition, which subse-

https://doi.org/10.1021/acsomega.3c07810
ACS Omega 2024, 9, 4613−4626

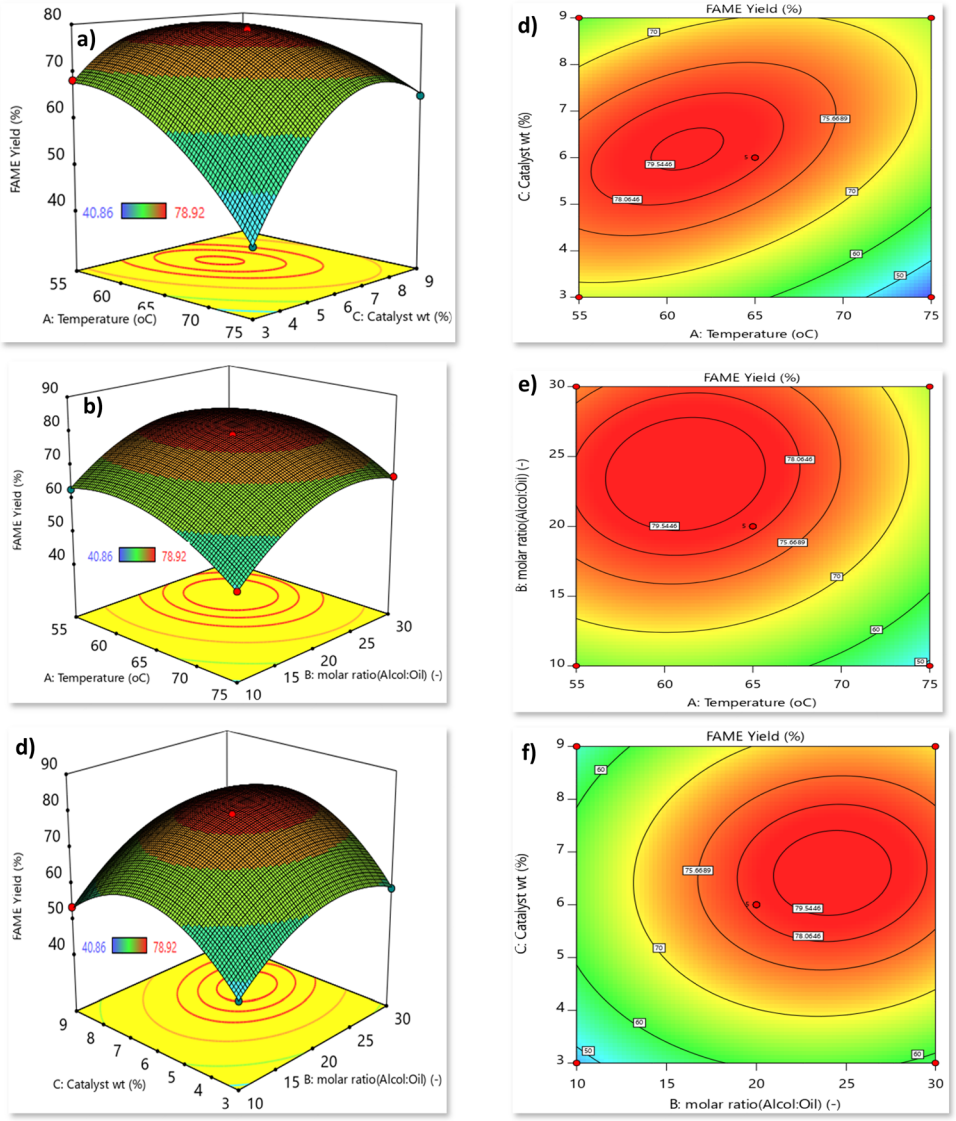

Figure 9. Three-dimensional and contour plots for the combined effects of reaction conditions: catalyst dosage with temperature interaction (a and d); interaction of temperature with methanol-to-oil molar ratio (b and c); interaction between methanol-to-oil molar ratio and catalyst dose (c and f).

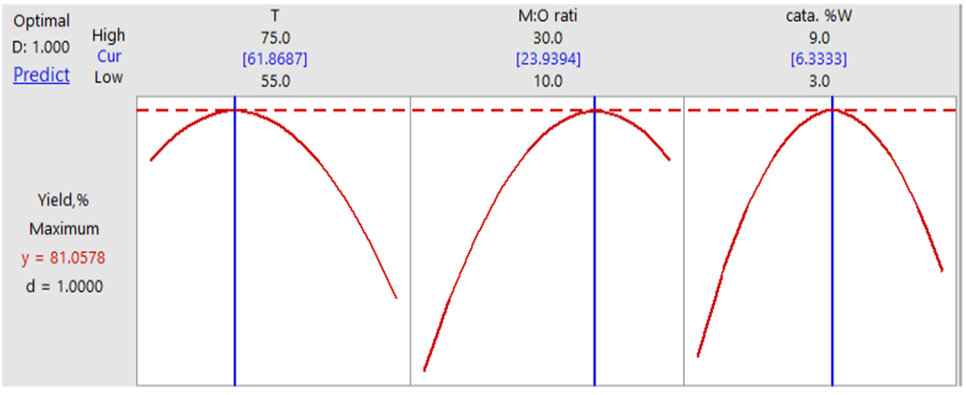

Figure 10. Optimization plots of yield.

quently impact the catalysis product being formed.[13] The optimal yield of FAME via the RC-ITB catalyst is therefore comparable to that of other previous solid-state catalysis research outputs. The dissimilarity between the various tabulated numbers might be related to the particle size, activation modes and composition of the catalyst source, reaction condition level optimization, and the kind of oil feedstock. Thus, it is interesting to note that residues of the

https://doi.org/10.1021/acsomega.3c07810
ACS Omega 2024, 9, 4613−4626

Table 6. Optimization Criteria and Validation Results at the Optimum Conditions

		limit			experimental value		
name	goal	lower	upper	predicted value	run 1	run 2	run 3
temperature,°C	in range	55	75	61.87	61 ± 2	61 ± 2	61 ± 2
methanol:oil molar ratio	in range	10	30	23.94	23.94	23.94	23.94
catalyst amount, wt %	in range	3	9	6.33	6.33	6.33	6.33
FAME yield, %	maximize	40.86	78.92	81.06	79.96	80.44	79.72
average yield					80.04		

Table 7. Comparison of the Optimum Yield with Other Heterogeneous Catalyzed Methanolysis Products

catalyst type	activation time and temperature (h, °C)	oil feedstock	FAME yield,%	references
RC-ITB	(3, 600)	waste cooking palm oil	80.04	this study
NaOH-loaded sepiolite	(5, 500)	canola oil	80.93	47
CaO nanocatalyst	(2, 400)	Green alga, *Chlorella vulgaris* oil	67	39
KNO3-loaded coffee husk ash	(2, 600)	waste frying oil valorization	72.04	24
zinc-doped CaO nanocatalyst	(3, 800)	Calophyllum inophyllum oil	89	25
fly ash	(2, 120)	mixture of purified palm plus waste frying oil	73.8	32
KOH/bentonite catalysts	(5, 400)	palm oil	90.7	48
OH-impregnated CaO	(2, 600)	refined coconut oil	81.70	8
ostrich bones derived catalyst	(4, 900)	waste cooking oil	90.56	26
strontium titanate	(8, 880)	Madhuca indica oil	98	49
walnut shell ash	(2, 800)	sunflower oil	98	36

reaction between calcium-hypochlorite and additional alkali activators to produce bleach in liquid form can also be used as precursors for the development of basic catalysts and have positive environmental effects.

Catalyst Reusability Test. For the reusability test, the catalyst separated from the reaction mixture under the optimum reaction conditions was subjected to its reusability test via a continual reaction of 4 cycles without any treatment. Figure 11 shows the dramatic reduction of yield over the successive reaction in the presence of the penultimately used catalyst. The continual decrease of yield, i.e, from 67.35 to 26.49%, may be due to the accumulation of WCO-derived organic byproducts and impurities onto the catalyst surface during the reactions. The attachment of impurities could be responsible for blocking the active sites and decreasing their catalytic activities.

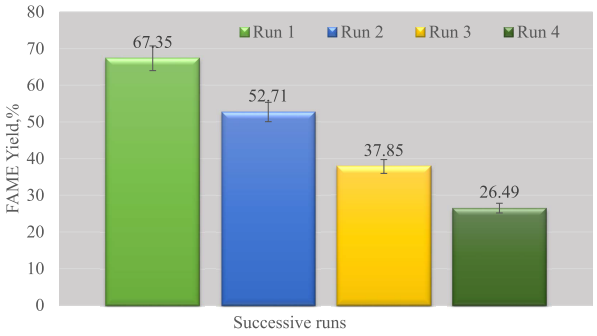

Figure 11. Reusability tests of the RC-ITB catalyst.

Catalyst Working Mechanism in the Transesterification Reaction. Basically, the route of biodiesel synthesis through transesterification involves interacting with the molecules of triglycerides and monohydric alcohols with the aid of a suitable catalyst. During this entire process, the triglyceride molecules are converted to a mixture of monoalkyl esters (biodiesel) by removing glycerol through three successive reaction steps that are reversible in nature (Scheme 1a); triglycerides undergo conversion to diglycerides, which then produce monoglycerides, and subsequently, monoalkyl esters (biodiesel) and glycerol are formed from monoglycerides. The entire reaction process is typically the sum of these steps, where 3 mol of alkyl esters and 1 mol of glycerol are produced because of the reaction between 1 mol of triglycerides and 3 mol of the alcohol reactant (Scheme 1b).

Furthermore, the alkaline traits of the prepared catalyst were logically verified with measurements of the pH and composition analysis. As a result, the catalyst's chemical activity during the reaction is thought of as a solid alkali-catalyzed procedure, as shown in Scheme 2. A methoxide ion acting as a strong nucleophile and a protonated catalyst is first produced by the surface interaction of methanol with the active species of alkaline catalyst $Z^{\delta+} - O^{\delta-}$ (Z = metal elements within the compound forms, such as $CaCO_3$, CaO, $Ca(OH)_2$, Na_2O, or K_2O).[24,50] In step 2, a reactive tetrahedral intermediate is produced when the methoxide attacks nucleophilically the triglyceride's carbonyl group, from which the Diglycerides anion and 1 mol of methyl ester are generated in step 3. In the fourth step, the diglyceride anion is neutralized by its protonation via deprotonation of the catalyst surface. Then, the catalyst can react with the second alcohol molecule for further catalysis until the remaining 2 mol of FAME is produced through the transformation of diglycerides and monoglycerides. The conversion and protonation mechanisms of diglycerides and monoglycerides on the catalyst surface are similar to those of triglycerides to form glycerol molecules and a combination of alkyl esters.

Fuel Properties. Table 8 presents the properties of the optimal methyl ester fuel derived from the WCO with respect to the limits of the international standard to be guaranteed for a minimum quality. The jelly and corrosive features of the biodiesel are commonly explained with its saponification and acid value, respectively. The acid value shows the presence of free fatty acids in the biodiesel and is quantitatively defined as the quantity of KOH necessary for neutralizing one gram of oil,

https://doi.org/10.1021/acsomega.3c07810
ACS Omega 2024, 9, 4613−4626

Scheme 1. Sequential (a) and Overall (b) Transesterification Mechanism of Triglycerides

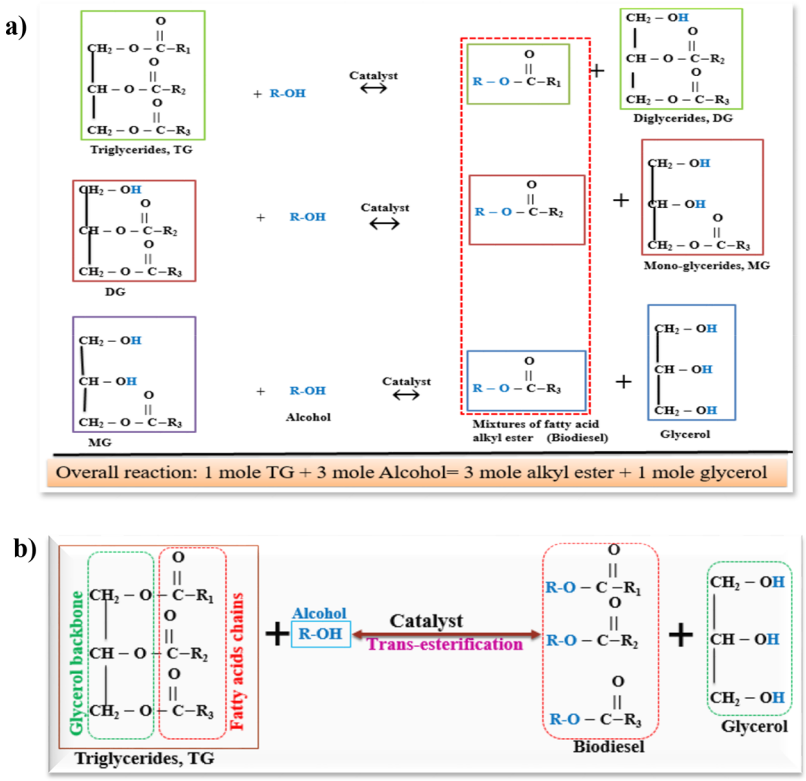

Scheme 2. Mechanism of the Transesterification Process on a Solid Alkali Catalyst Surface

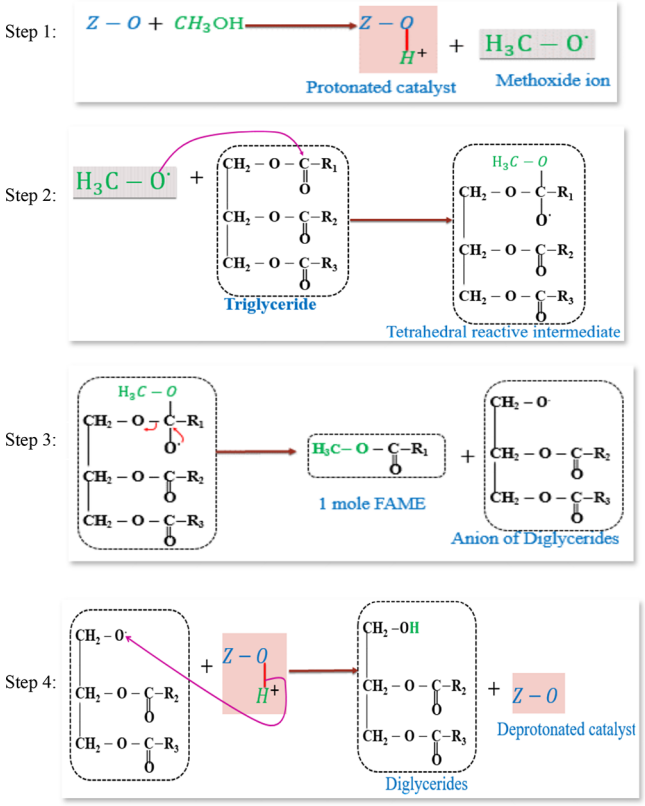

while the saponification number signifies the quantity of KOH in milligrams wanted to saponify one gram of sample.[3,51] Due to the methanolysis reaction, their values have been soundly decreased from the waste cooking oil feedstock and acceptably within the ASTM D6751 limits.

Table 8. Waste Cooking-Oil-Derived Biodiesel Fuel Properties

			standard limits biodiesel	
quality parameters	unit	test result	ASTM D6751	EN 14214
acid value	mg KOH g^{-1}	0.77	<0.8	≤0.5
kinematic viscosity at 40 °C	mm^2 s^{-1}	4.91	1.9−6.0	3.5−5.0
saponification number	mg KOH g^{-1}	136.72	370 max	
cetane number		30.2	≥47	≥51
cloud point	°C	4.66	−3.0 to 12	
pour point	°C	−1.33	−15 to 16	
S.G at 15 °C		0.876	0.87−0.98	
density at 15 °C	kg m^{-3}	875.1	max 880	860−900

One of the most essential quality indications of the fuel's ignition delay is the cetane number, which is influenced by composition. The larger the cetane number, the greater the combustibility and shorter ignition delay.[3,52,53] Conversely, lower CN leads to hard starting which affects ignition delay, rough operation, noise, and emissions of particulate matter (PM), NO_X, and hydrocarbons. The result of cetane number determination was about 30.2, which is smaller than ASTM D6751 and EN 14214 limits, most likely due to the aromaticity and presence of unsaturation in the biodiesel.[53] As aniline is the simplest aromatic amine, it was totally mixed with the biodiesel sample at an atmospheric temperature in the period

https://doi.org/10.1021/acsomega.3c07810
ACS Omega 2024, 9, 4613−4626

of the test, which suggests the aromaticity of biodiesel exhibited lower cetane number.

The traits of the waste cooking oil-based biodiesel flow in a cold atmosphere were analyzed in terms of both pour and cloud points. The cloud point is the level of temperature that occurs when atomic compacting is initiated due to the formation of visible wax-like when the biodiesel is refrigerated; below the cloud point, larger crystals fused together that eventually become enough to prevent pouring. The pour point is then the smallest temperature whereby the flow characteristics of the biodiesel are lost; biodiesel is no longer pumpable at this temperature, and thus the fuel is appropriate for applications exceeding the pour point.[3,52,54,55] The results of 4.66 °C (cloud point) and −1.33 °C (pour point) met the ASTM D6751 standards. The flow characteristics of the biodiesel are explained in terms of the mass per unit volume (density) and resistance to flow (kinematic viscosity). When their values became larger, the creation of engine sediments, large injection pressures, inadequate spray, inadequate combustion, and unequal distribution in to the cylinder could be resulted. The blending of conventional fuels with biodiesel is commonly recommended for improved combustion efficacy in diesel engines.[5,43] Their experimental values were 875.1 kg/m^3 and 4.91 mm^2/s, respectively, which are both adequately within the standard.

FT-IR Analysis of Waste Cooking Oil Methyl Ester. The shifting of WCO into the corresponding FAME was confirmed with FTIR spectroscopy by chemically mapping components in a specific wavelength range within the sample. Most of the fundamental distinctive bands that compose biodiesel are found in the area known as the fingerprint within the range of 1400 and 600 cm^{-1}.[5,56] Many of the prominent bands on biodiesel and WCO represent the same functional groups, irrespective of being weak and/or strong bands (Table 9 and Figure 12). However, a perfect difference between the biodiesel and WCO is observed in the fingerprint region, particularly at around 1016 cm^{-1} because of the methoxyl group (O−CH$_3$) substitution for the cracked glycerol backbone of the WCO in the biodiesel. Furthermore, the wider OH-stretching bans of WCO are changed to a nearly straight line in the biodiesel because of the substrate acid value reduction through the transesterification reaction.

Table 9. Principal Bands of Waste Cooking Oil and Biodiesel

chemical group and bond type	mode of vibration	~ wavenumber, cm^{-1} biodiesel (FAME)	WCO
moisture, carboxylic acid and alcohol (O−H)	stretching	3473	3473
alkenes and aromatics (=C−H)	stretching	3006	3006
aliphatics (asymmetric C−H)	stretching	2923	2930
aliphatics (symmetric C−H)	stretching	2854	2844
ketones, ester, aldehydes (C−O)	stretching	1744	1748
alkane (C−H in −CH$_3$− and −CH$_2$−)	bending	1458	1459
alkane (C−H in −CH$_3$)	bending	1362	1374
ester (asymmetric C−O in C−C(=O)−O)	stretching	1168	1168
ester (asymmetric C−O in O−C−C)	stretching	1115	1112
aromatic (C−H)	bending	874	870
alkane (C−H)	rocking	723	722

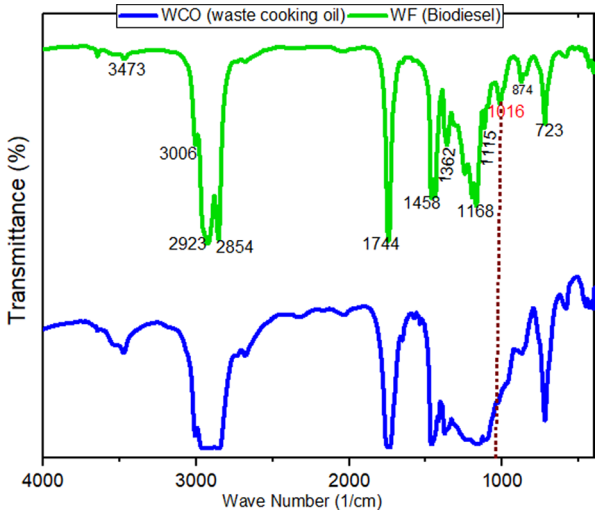

Figure 12. FT-IR spectra of waste cooking oil with its biodiesel.

CONCLUSIONS

In the present work, the potential of NaOH-impregnated sediments from commercial household bleach-making to catalyze waste-cooking-oil methanolysis was introduced. The analysis results of the prepared catalyst (RC-ITB) showed 9.312 m^2 g^{-1} of the BET area and the maximum concentration of calcium with its compound forms like carbonates, hydroxides, and oxides were perceived as the most likely components of alkali solid catalysts that contain calcium. Also, the evaluation of basic character revealed RC-ITB has improved alkalinity with a pH value of 12.65 relative to its precursor RC (pH = 10.66) at the same dilution ratio, primarily caused by OH infusion. The interaction impacts of temperature, catalyst dosage, and molar ratio on the yield of FAME variations were assessed, and the RSM approach was realized for optimization. Hence, the optimum response of 80.04% was obtained at the reaction conditions combination of temperature 61 ± 2 °C, molar ratio 23.94, and catalyst load 6.33%. A test for catalyst reusability was conducted in a continuous reaction of four cycles without any treatment at the optimal reaction conditions; accordingly, a gradual reduction in yield was observed from the successive reactions since the buildup of organic impurities on the catalyst surface blocked its active sites and decreased catalytic activity. The product's fuel characteristics were assessed and found to comply with ASTM D6751 criteria, excluding the cetane number. Moreover, the replacement of the glycerol part of WCO with methoxyl units to form the equivalent FAME product was proven through the FTIR method. In general, the above-mentioned sediments have been effectively attested for basic solid catalyst development, which might have industrial as well as scholarly significance in the future.

ASSOCIATED CONTENT

Supporting Information

The Supporting Information is available free of charge at https://pubs.acs.org/doi/10.1021/acsomega.3c07810.

Details of chemical and equipment lists; photographic outlook of catalyst preparation; catalyst characterization

https://doi.org/10.1021/acsomega.3c07810
ACS Omega 2024, 9, 4613−4626

methods; detail XRF results; and reaction procedures (PDF)

AUTHOR INFORMATION

Corresponding Author

Kedir Derbie Mekonnen − *School of Mechanical and Chemical Engineering, Kombolcha Institute of Technology, Wollo University, Wollo 208, Ethiopia;* orcid.org/0000-0001-9612-9324; Phone: +251 925216653; Email: kedirched@gmail.com, kedirched@kiot.edu.et

Author

Anwar Yimer Yesuf − *School of Mechanical and Chemical Engineering, Kombolcha Institute of Technology, Wollo University, Wollo 208, Ethiopia*

Complete contact information is available at: https://pubs.acs.org/10.1021/acsomega.3c07810

Author Contributions

The manuscript was written through contributions of both authors. Both authors have given approval to the final version of the manuscript.

Notes

The authors declare no competing financial interest.

ACKNOWLEDGMENTS

The authors acknowledge the financial support of Kombolcha Institute of Technology, Wollo University, Ethiopia (https://kiot.wu.edu.et/).

ABBREVIATIONS

FTIR	Fourier transform infrared spectroscopy
SEM	Scanning electron microscopy
XRD	X-ray diffraction
XRF	X-ray fluorescence
BET	Brunauer−Emmet−Teller
DSC	Differential scanning calorimeter
AV	Acid value
FFA	Free fatty acid
FoM	Figure of merit
SV	Saponification values
WCO	Waste cooking palm oil
MW	Molecular weight
FAME	Fatty acid methyl ester
ASTM	American Standard for Testing Material
RSM	Response surface methodology
ANOVA	Analysis of variance

REFERENCES

(1) Arazo, R. O.; Luna, M. D. G.; Capareda, S. C. Assessing Biodiesel Production from Sewage Sludge-Derived Bio-Oil. *Biocatal. Agric. Biotechnol.* **2017**, *10*, 189−196.

(2) Dharma, S.; Masjuki, H. H.; Chyuan, H.; Sebayang, A. H.; Silitonga, A. S.; Kusumo, F.; Mahlia, T. M. I. Optimization of Biodiesel Production Process for Mixed Jatropha Curcas − Ceiba Pentandra Biodiesel Using Response Surface Methodology. *Energy Convers. Manag.* **2016**, *115*, 178−190.

(3) Singh, D.; Sharma, D.; Soni, S. L.; Sharma, S.; Kumari, D. Chemical Compositions, Properties, and Standards for Different Generation Biodiesels: A Review. *Fuel* **2019**, *253*, 60−71.

(4) Maneechakr, P.; Karnjanakom, S. A Combination of 2k Factorial with Box-Behnken Designs for FAME Production via Methanolysis of Waste Cooking Palm Oil over Low-Cost Catalyst. *J. Environ. Chem. Eng.* **2019**, *7* (5), No. 103389.

(5) Mekonnen, K. D.; Sendekie, Z. B. NaOH-Catalyzed Methanolysis Optimization of Biodiesel Synthesis from Desert Date Seed Kernel Oil. *ACS. Omega* **2021**, *6* (37), 24082−24091.

(6) Leung, D. Y. C.; Wu, X.; Leung, M. K. H. A Review on Biodiesel Production Using Catalyzed Transesterification. *Applied Energy* **2010**, *87* (4), 1083−1095.

(7) Tariq, M.; Ali, S.; Khalid, N. Author's Personal Copy Activity of Homogeneous and Heterogeneous Catalysts, Spectroscopic and Chromatographic Characterization of Biodiesel: A Review. *Renew. Sustainable Energy Rev.* **2012**, *16*, 6303−6316, DOI: 10.1016/j.rser.2012.07.005.

(8) Bambase, M. E.; Almazan, R. A. R.; Demafeils, R. B.; Sobremisana, M. J.; Dizon, L. S. Biodiesel Production from Re Fi Ned Coconut Oil Using Hydroxide-Impregnated Calcium Oxide by Cosolvent Method. *Renew. Energy* **2021**, *163*, 571−578.

(9) Huang, W.; Tang, S.; Zhao, H.; Tian, S. Activation of Commercial CaO for Biodiesel Production from Rapeseed Oil Using a Novel Deep Eutectic Solvent. *Ind. Eng. Chem. Res.* **2013**, *52*, 11943−11947.

(10) Mutreja, V.; Singh, S.; Ali, A. Biodiesel from Mutton Fat Using KOH Impregnated MgO as Heterogeneous Catalysts. *Renewable Energy* **2011**, *36* (8), 2253−2258.

(11) Bedir, Ö.; Doğan, T. H. Environmental Effects Comparison of Catalytic Activities of Ca-Based Catalysts from Waste in Biodiesel Production. *Energy Sources* **2021**, *00* (00), 1−18.

(12) Mat, R.; Samsudin, R. A.; Mohamed, M.; Johari, A. Solid Catalysts and Their Application in Biodiesel Production. *Bulletin of Chemical Reaction Engineering and Catalysis* **2012**, *7* (2), 142−149.

(13) Sronsri, C.; Sittipol, W.; U-yen, K. Performance of CaO Catalyst Prepared from Magnetic-Derived CaCO 3 for Biodiesel Production. *Fuel* **2021**, *304*, No. 121419.

(14) Si, J.; Ling, J.; Hua, Y.; Nabisab, T.; Mubarak, M.; Kansedo, J.; Saptoro, A.; Hipolito, C. N. A Review of Heterogeneous Calcium Oxide Based Catalyst from Waste for Biodiesel Synthesis. *SN Appl. Sci.* **2019**, *1*, 810.

(15) Mandari, V.; Kumar, S. Biodiesel Production Using Homogeneous, Heterogeneous, and Enzyme Catalysts via Transesterification and Esterification Reactions: A Critical Review. *BioEnergy Res.* **2022**, *15*, 935−961.

(16) Marinkovi, D. M.; Stankovi, M. V.; Veli, A. V.; Avramovi, J. M.; Miladinovi, M. R.; Stamenkovi, O. O.; Veljkovi, V. B.; Jovanovi, M. Calcium Oxide as a Promising Heterogeneous Catalyst for Biodiesel Production: Current State and Perspectives. *Renew. Sustainable Energy Rev.* **2016**, *56*, 1387−1408.

(17) Abdullah, S. H. Y. S.; Hanapi, N. H. M.; Azid, A.; Umar, R.; Juahir, H.; Khatoon, H.; Endut, A. A Review of Biomass-Derived Heterogeneous Catalyst for a Sustainable Biodiesel Production. *Renewable and Sustainable Energy Reviews* **2017**, *70*, 1040−1051.

(18) Smith, L. Historical Perspectives on Water Purification. In *Chemistry and Water*; Elsevier Inc., 2017; pp. 421−468.

(19) Hussain, T. *Bleaching and Dyeing of Jute*, 2016.

(20) Anand, S. S.; Philip, B. K.; Mehendale, H. M.; Anand, S. S.; Haskell, D.; Centers, G.; Sciences, E. Chlorination Byproducts. In *Encyclopedia of Toxicology*; Elsevier, 2014; Vol. *1*, pp. 855-859.

(21) Aamir, M.; Khan, N. A.; Ahmed, S.; Husain, A.; Hussain, A.; Changani, F.; Youse, M. Chlorination Disinfection By-Products in Municipal Drinking Water - A Review. *J. Cleaner Prod.* **2020**, *273*, No. 123159.

(22) Li, X. F.; Mitch, W. A. Drinking Water Disinfection Byproducts (DBPs) and Human Health Effects: Multidisciplinary Challenges and Opportunities. *Environ. Sci. Technol.* **2018**, *52* (4), 1681−1689.

(23) Ropp, R. C. Group 17 (H, F, Cl, Br, I) Alkaline Earth Compounds. In *Encyclopedia of the Alkaline Earth Compounds*; Elsevier, 2013; Vol. *17*, pp. 25−104.

(24) Bekele, D. T.; Shibeshi, N. T.; Reshad, A. S. KNO3-Loaded Coffee Husk Ash as a Heterogeneous Alkali Catalyst for Waste Frying Oil Valorization into Biodiesel. *ACS Omega* **2022**, *7*, 45129−45143.

https://doi.org/10.1021/acsomega.3c07810
ACS Omega 2024, 9, 4613−4626

(25) Naveenkumar, R.; Baskar, G. Biodiesel Production from Calophyllum Inophyllum Oil Using Zinc Doped Calcium Oxide (Plaster of Paris) Nanocatalyst. *Bioresour. Technol.* **2019**, *280*, 493−496.
(26) Mahmood Khan, H.; Iqbal, T.; Haider Ali, C.; Javaid, A.; Iqbal Cheema, I. Sustainable Biodiesel Production from Waste Cooking Oil Utilizing Waste Ostrich (Struthio Camelus) Bones Derived Heterogeneous Catalyst. *Fuel* **2020**, *277*, No. 118091.
(27) Ayoola, A. A.; Fayomi, O. S. I.; Usoro, I. F. Data on PKO Biodiesel Production Using CaO Catalyst from Turkey Bones. *Data in Brief* **2018**, *19*, 789−797.
(28) Basumatary, B.; Das, B.; Nath, B.; Basumatary, S. Synthesis and Characterization of Heterogeneous Catalyst from Sugarcane Bagasse: Production of Jatropha Seed Oil Methyl Esters. *Current Research in Green and Sustainable Chemistry* **2021**, *4*, No. 100082.
(29) Basumatary, B.; Basumatary, S.; Das, B.; Nath, B. Waste Musa Paradisiaca Plant: An Ef Fi Cient Heterogeneous Base Catalyst for Fast Production of Biodiesel. *J. Cleaner Prod.* **2021**, *305*, No. 127089.
(30) Mo, M.; Masjuki, H. H.; Kalam, M. A.; Atabani, A. E. Evaluation of Biodiesel Blending, Engine Performance and Emissions Characteristics of Jatropha Curcas Methyl Ester: Malaysian Perspective. *Energy* **2013**, *55*, 879−887.
(31) Ngoya, T.; Aransiola, E. F.; Oyekola, O. Optimisation of Biodiesel Production from Waste Vegetable Oil and Eggshell Ash. *South Afr. J. Chem. Eng.* **2017**, *23*, 145 DOI: 10.1016/j.sajce.2017.05.003.
(32) Vargas, E. M.; Ospina, L.; Neves, M. C.; Tarelho, L. A. C.; Nunes, M. I. Optimization of FAME Production from Blends of Waste Cooking Oil and Refined Palm Oil Using Biomass Fly Ash as a Catalyst. *Renewable Energy* **2021**, *163*, 1637−1647.
(33) El Bakkari, M.; Bindiganavile, V.; Boluk, Y. Facile Synthesis of Calcium Hydroxide Nanoparticles onto TEMPO-Oxidized Cellulose Nanofibers for Heritage Conservation. *ACS Omega* **2019**, *4*, 20606−20611.
(34) Hassid, A.; Klinger, M.; Cohen, H. TGA − DSC Combined Coal Analysis as a Tool for QC (Quality Control) and Reactivity Patterns of Coals. *ACS Omega* **2022**, *7*, 1893−1907.
(35) Yi, L.; Liu, H.; Li, M.; Man, G.; Yao, H. Prevention of CaO Deactivation Using Organic Calcium Precursor during Multicyclic Catalytic Upgrading of Bio-Oil. *Fuel* **2020**, *271*, No. 117692.
(36) Miladinovi, M. R.; Krsti, J. B.; Stamenkovi, O. S. Valorization of Walnut Shell Ash as a Catalyst for Biodiesel Production. *Renew. Energy* **2020**, *147*, 1033−1043.
(37) Mosaddegh, E.; Hassankhani, A. Preparation and Characterization of Nano - CaO Based on Eggshell Waste: Novel and Green Catalytic Approach to Highly Efficient Synthesis of Pyrano [4, 3 - b] Pyrans. *Chinese Journal of Catalysis* **2014**, *35* (3), 351−356.
(38) Laohavisuti, N.; Boonchom, B.; Boonmee, W. *Simple Recycling of Biowaste Eggshells to Various Calcium Phosphates for Specific Industries*; Nature Publishing Group: UK, 2021.
(39) Davoodbasha, M.; Pugazhendhi, A.; Kim, J.; Lee, S. Biodiesel Production through Transesterification of Chlorella Vulgaris: Synthesis and Characterization of CaO Nanocatalyst. *Fuel* **2021**, *300*, No. 121018.
(40) Pour, N. E.; Dumeignil, F.; Katryniok, B.; Delevoye, L.; Revel, B. Investigating the Active Phase of Ca-Based Glycerol Polymerization Catalysts: On the Importance of Calcium Glycerolate. *Mol. Catal.* **2021**, *507*, No. 111571.
(41) Olubunmi, B. E.; Karmakar, B.; Aderemi, O. M.; Auta, M.; Halder, G. Parametric Optimization by Taguchi L9 Approach towards Biodiesel Production from Restaurant Waste Oil Using Fe-Supported Anthill Catalyst. *J. Environ. Chem. Eng.* **2020**, *8* (5), No. 104288.
(42) Lee, H. V.; Yunus, R.; Juan, J. C.; Tau, Y. H. Process Optimization Design for Jatropha-Based Biodiesel Production Using Response Surface Methodology. *Fuel Process. Technol.* **2011**, *92*, 2420−2428.
(43) Ogunkunle, O.; Oniya, O. O.; Adebayo, A. O. Yield Response of Biodiesel Production from Heterogeneous and Homogeneous Catalysis of Milk Bush Seed (Thevetia Peruviana) Oil. *Energy and Policy Research* **2017**, *4* (01), 21−28.
(44) Mathiyazhagan, M.; Ganapathi, A. Factors Affecting Biodiesel Production. *Res. Plant Biol.* **2011**, *1* (2), 1−5.
(45) Parawira, W. Biodiesel Production from Jatropha Curcas: A Review Biodiesel Production from Jatropha Curcas: A Review. *Sci. Res. Essays* **2014**, *5* (14), 1796−1808.
(46) Meher, L. C.; Sagar, D. V.; Naik, S. N. Technical Aspects of Biodiesel Production by Transesterification — a Review. *Renew. Sustainable Energy Rev.* **2006**, *10*, 248−268.
(47) Aslan, S.; Aka, N.; Karaoglu, M. H. NaOH Impregnated Sepiolite Based Heterogeneous Catalyst and Its Utilization for the Production of Biodiesel from Canola Oil. *Energy Sources A* **2019**, *41* (3), 290−297.
(48) Soetaredjo, F. E.; Ayucitra, A.; Ismadji, S.; Maukar, A. L. KOH/Bentonite Catalysts for Transesterification of Palm Oil to Biodiesel. *Appl. Clay Sci.* **2011**, *53* (2), 341−346.
(49) Sahani, S.; Roy, T.; Sharma, Y. C. Studies on Fast and Green Biodiesel Production from an Indigenous Nonedible Indian Feedstock Using Single Phase Strontium Titanate Catalyst. *Energy Conversion and Management* **2020**, *203*, No. 112180.
(50) Bhuiya, M. M. K.; Rasul, M. G.; Khan, M. M. K.; Ashwath, N.; Azad, A. K. Prospects of 2nd Generation Biodiesel as a Sustainable Fuel — Part: 1 Selection of Feedstocks, Oil Extraction Techniques and Conversion Technologies. *Renew. Sustainable Energy Rev.* **2015**, *55*, 1109−1128.
(51) Kumar, R.; Kumar, V.; Sham, R. Stability of Biodiesel − A Review. *Renew. Sustainable Energy Rev.* **2016**, *62*, 866−881.
(52) Sani, S.; Kaisan, M. U.; Kulla, D. M.; Obi, A. I.; Jibrin, A.; Ashok, B. Industrial Crops & Products Determination of Physico Chemical Properties of Biodiesel from Citrullus Lanatus Seeds Oil and Diesel Blends. *Industrial Crops & Products* **2018**, *122*, 702−708.
(53) Nalgundwar, A.; Paul, B.; Sharma, S. K. Comparison of Performance and Emissions Characteristics of Di CI Engine Fueled with Dual Biodiesel Blends of Palm and Jatropha. *Fuel* **2016**, *173*, 172−179.
(54) Hoekman, S. K.; Broch, A.; Robbins, C.; Ceniceros, E.; Natarajan, M. Review of Biodiesel Composition, Properties, and Specifications. *Renewable and Sustainable Energy Reviews* **2012**, *16* (1), 143−169.
(55) Naureen, R.; Tariq, M.; Yusoff, I.; Chowdhury, A. J. K.; Ashraf, M. A. Synthesis, Spectroscopic and Chromatographic Studies of Sunflower Oil Biodiesel Using Optimized Base Catalyzed Methanolysis. *Saudi Journal of Biological Sciences* **2015**, *22* (3), 332−339.
(56) Mekonnen, K. D. Fourier Transform Infrared Spectroscopy as a Tool for Identifying the Unique Characteristic Bands of Lipid in Oilseed Components: Confirmed via Ethiopian Indigenous Desert Date Fruit. *Heliyon* **2023**, *9* (4), No. e14699.

https://doi.org/10.1021/acsomega.3c07810
ACS Omega 2024, 9, 4613−4626